
Are Disentangled Representations Helpful for Abstract Visual Reasoning?

Sjoerd van Steenkiste
IDSIA, USI, SUPSI
sjoerd@idsia.ch

Francesco Locatello
ETH Zurich, MPI-IS
locatelf@ethz.ch

Jürgen Schmidhuber
IDSIA, USI, SUPSI, NNAISENSE
juergen@idsia.ch

Olivier Bachem
Google Research, Brain Team
bachem@google.com

Abstract

A disentangled representation encodes information about the salient factors of variation in the data independently. Although it is often argued that this representational format is useful in learning to solve many real-world up-stream tasks, there is little empirical evidence that supports this claim. In this paper, we conduct a large-scale study that investigates whether disentangled representations are more suitable for abstract reasoning tasks. Using two new tasks similar to Raven’s Progressive Matrices, we evaluate the usefulness of the representations learned by 360 state-of-the-art unsupervised disentanglement models. Based on these representations, we train 3600 abstract reasoning models and observe that disentangled representations do in fact lead to better up-stream performance. In particular, they appear to enable quicker learning using fewer samples.

1 Introduction

Learning good representations of high-dimensional sensory data is of fundamental importance to Artificial Intelligence [4, 3, 6, 48, 7, 67, 65, 49, 57, 71]. In the supervised case, the quality of a representation is often expressed through the ability to solve the corresponding up-stream task. However, in order to leverage vast amounts of unlabeled data, we require a set of desiderata that apply to more general real-world settings.

Following the successes in learning *distributed* representations that efficiently encode the content of high-dimensional sensory data [44, 54, 73], recent work has focused on learning representations that are *disentangled* [6, 67, 66, 71, 69, 26, 27, 42, 10, 61, 16, 50, 51, 47, 9]. A disentangled representation captures information about the salient (or explanatory) factors of variation in the data, isolating information about each specific factor in only a few dimensions. Although the precise circumstances that give rise to disentanglement are still being debated, the core concept of a local correspondence between data-generative factors and learned latent codes is generally agreed upon [16, 26, 50, 61, 69].

Disentanglement is mostly about *how* information is encoded in the representation, and it is often argued that a representation that is disentangled is desirable in learning to solve challenging real-world up-stream tasks [6, 71, 57, 7, 26, 66]. Indeed, in a disentangled representation information about an individual factor value can be readily accessed and is robust to changes in the input that do not affect this factor. Hence, learning to solve an up-stream task from a disentangled representation is expected to require fewer samples and be easier in general [66, 6, 28, 29, 57]. Moreover, many real-world generative processes are based on latent spaces that factorize. Hence, disentangled

representations that capture this product space are expected to help in generalizing systematically in this regard [18, 22, 57].

Several of these purported benefits can be traced back to empirical evidence presented in the recent literature. Disentangled representations have been found to be more sample-efficient [29], less sensitive to nuisance variables [53], and better in terms of (systematic) generalization [1, 16, 28, 35, 68]. However, in other cases it is less clear whether the observed benefits are actually due to disentanglement [47]. Indeed, while these results are generally encouraging, a systematic evaluation on a complex up-stream task of a wide variety of disentangled representations obtained by training different models, using different hyper-parameters and data sets appears to be lacking.

Contributions In this work, we conduct a large-scale evaluation¹ of disentangled representations to systematically evaluate some of these purported benefits. Rather than focusing on a simple single factor classification task, we evaluate the usefulness of disentangled representations on abstract visual reasoning tasks that challenge the current capabilities of state-of-the-art deep neural networks [30, 63]. Our key contributions include:

- We create two new visual abstract reasoning tasks similar to Raven’s Progressive Matrices [59] based on two disentanglement data sets: *dSprites* [27], and *3dshapes* [42]. A key design property of these tasks is that they are hard to solve based on statistical co-occurrences and require reasoning about the relations between different objects.
- We train 360 unsupervised disentanglement models spanning four different disentanglement approaches on the individual images of these two data sets and extract their representations. We then train 3600 Wild Relation Networks [63] that use these disentangled representations to perform abstract reasoning and measure their accuracy at various stages of training.
- We evaluate the usefulness of disentangled representations by comparing the accuracy of these abstract reasoning models to the degree of disentanglement of the representations (measured using five different disentanglement metrics). We observe compelling evidence that more disentangled representations yield better sample-efficiency in learning to solve the considered abstract visual reasoning tasks. In this regard our results are complementary to a recent prior study of disentangled representations [50] that did not find evidence of increased sample efficiency on a much simpler up-stream task.

2 Background and Related Work on Learning Disentangled Representations

Despite an increasing interest in learning disentangled representations, a precise definition is still a topic of debate [16, 26, 50, 61]. In recent work, Eastwood et al. [16] and Ridgeway et al. [61] put forth three criteria of disentangled representations: *modularity*, *compactness*, and *explicitness*. Modularity implies that each code in a learned representation is associated with only one factor of variation in the environment, while compactness ensures that information regarding a single factor is represented using only one or few codes. Combined, modularity and compactness suggest that a disentangled representation implements a one-to-one mapping between salient factors of variation in the environment and the learned codes. Finally, a disentangled representation is often assumed to be explicit, in that the mapping between factors and learned codes can be implemented with a simple (i.e. linear) model. While modularity is commonly agreed upon, compactness is a point of contention. Ridgeway et al. [61] argue that some features (eg. the rotation of an object) are best described with multiple codes although this is essentially not compact. The recent work by Higgins et al. [26] suggests an alternative view that may resolve these different perspectives in the future.

Metrics Multiple metrics have been proposed that leverage the ground-truth generative factors of variation in the data to measure disentanglement in learned representations. In recent work, Locatello et al. [50] studied several of these metrics, which we will adopt for our purposes in this work: the *BetaVAE* score [27], the *FactorVAE* score [42], the *Mutual Information Gap (MIG)* [10], the disentanglement score from Eastwood et al. [16] referred to as the *DCI disentanglement* score, and the *Separated Attribute Predictability (SAP)* score [47].

¹Reproducing these experiments requires approximately 2.73 GPU years (NVIDIA P100).

The *BetaVAE* score, *FactorVAE* score, and *DCI disentanglement* score focus primarily on *modularity*. The former assess this property through *interventions*, i.e. by keeping one factor fixed and varying all others, while the *DCI disentanglement* score estimates this property from the relative importance assigned to each feature by a random-forest regressor in predicting the factor values. The *SAP* score and *MIG* are mostly focused on *compactness*. The *SAP* score reports the difference between the top two most predictive latent codes of a given factor, while *MIG* reports the difference between the top two latent variables with highest mutual information to a certain factor.

The degree of *explicitness* captured by any of the disentanglement metrics remain unclear. In prior work it was found that there is a positive correlation between disentanglement metrics and up-stream performance on single factor classification [50]. However, it is not obvious whether disentangled representations are useful for up-stream performance per se, or if the correlation is driven by the explicitness captured in the scores. In particular, the *DCI disentanglement* score and the *SAP* score compute disentanglement by training a classifier on the representation. The former uses a random forest to extract feature importance in the representation, and the latter considers the gap in prediction accuracy of a support vector machine trained on each dimension of the representation to predict each factor of variation. *MIG* is based on the matrix of pairwise mutual information between factors of variations and dimensions of the representation, which also relates to the explicitness of the representation. On the other hand, the *BetaVAE* and *FactorVAE* scores predict the index of a fixed factors of variation and not the exact value.

Methods Several methods have been proposed to learn disentangled representations. Here we are interested in evaluating the benefits of disentangled representations that have been learned through *unsupervised* learning. In order to control for potential confounding factors that may arise in using a single model, we use the representations learned from four state-of-the-art approaches from the literature: *β -VAE* [27], *FactorVAE* [42], *β -TCVAE* [10], and *DIP-VAE* [47]. A similar choice of models was used in a recent study by Locatello et al. [50].

Using notation from Tschannen et al. [71], we can view all of these models as Auto-Encoders that are trained with the regularized variational objective of the form:

$$\mathbb{E}_{p(x)}[\mathbb{E}_{q_\phi(z|x)}[-\log p_\theta(x|z)]] + \lambda_1 \mathbb{E}_{p(x)}[R_1(q_\phi(z|x))] + \lambda_2 R_2(q_\phi(z)) \quad (1)$$

The output of the *encoder* that parametrizes $q_\phi(z|x)$ yields the representation. Regularization serves to control the information flow through the bottleneck induced by the encoder, while different regularizers primarily vary in the notion of disentanglement that they induce. *β -VAE* restricts the capacity of the information bottleneck by penalizing the KL-divergence, using $\beta = \lambda_1 > 1$ with $R_1(q_\phi(z|x)) := D_{KL}[q_\phi(z|x)||p(z)]$, and $\lambda_2 = 0$; *FactorVAE* penalizes the Total Correlation [74] of the latent variables via adversarial training, using $\lambda_1 = 0$ and $\lambda_2 = 1$ with $R_2(q_\phi(z)) := TC(q_\phi(z))$; *β -TCVAE* also penalizes the Total Correlation but estimates its value via a biased Monte Carlo estimator; and finally *DIP-VAE* penalizes a mismatch in moments between the aggregated posterior and a factorized prior, using $\lambda_1 = 0$ and $\lambda_2 \geq 1$ with $R_2(q_\phi(z)) := \|\text{Cov}_{q_\phi(z)} - I\|_F^2$.

Other related works Learning disentangled representations is similar in spirit to non-linear ICA, although it relies primarily on (architectural) inductive biases and different degrees of supervision [13, 2, 39, 36, 37, 38, 25, 33, 32]. Due to the initial poor performance of purely unsupervised methods, the field initially focused on semi-supervised [60, 11, 55, 56, 43, 45] and weakly supervised approaches [31, 12, 40, 21, 75, 20, 15, 35, 77, 52, 46, 62, 8]. In this paper, we consider the setup of the recent unsupervised methods [27, 26, 47, 42, 9, 50, 69, 10]. Finally, while this paper focuses on evaluating the benefits of disentangled *features*, these are complementary to recent work that focuses on the unsupervised “disentangling” of images into compositional primitives given by object-like representations [17, 23, 24, 22, 58, 72]. Disentangling pose, style, or motion from content are classical vision tasks that has been studied with different degrees of supervision [70, 76, 77, 34, 19, 14, 21, 36].

3 Abstract Visual Reasoning Tasks for Disentangled Representations

In this work we evaluate the purported benefits of disentangled representations on abstract visual reasoning tasks. Abstract reasoning tasks require a learner to infer abstract relationships between

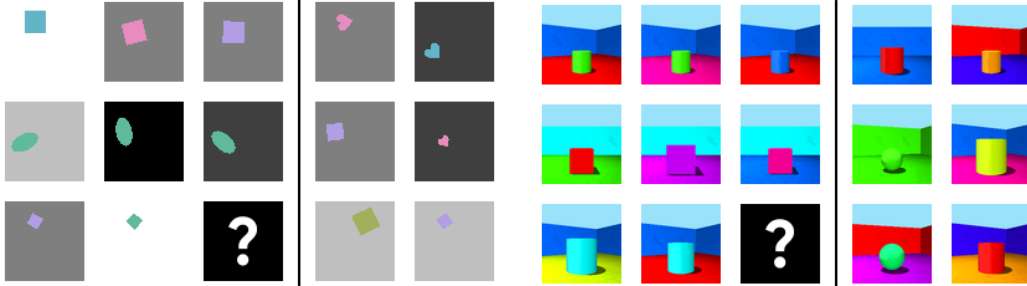


Figure 1: Examples of RPM-like abstract visual reasoning tasks using *dSprites* (left) and *3dshapes* (right). The correct answer and additional samples are available in Figure 18 in Appendix C.

multiple entities (i.e. objects in images) and re-apply this knowledge in newly encountered settings [41]. Humans are known to excel at this task, as is evident from experiments with simple visual IQ tests such as Raven’s Progressive Matrices (RPM) [59]. An RPM consists of several context panels organized in multiple sequences, with one sequence being incomplete. The task consists of completing the final sequence by choosing from a given set of answer panels. Choosing the correct answer panel requires one to infer the relationships between the panels in the complete context sequences, and apply this knowledge to the remaining partial sequence.

In recent work, Santoro et al. [63] evaluated the abstract reasoning capabilities of deep neural networks on this task. Using a data set of RPM-like matrices they found that standard deep neural network architectures struggle at abstract visual reasoning under different training and generalization regimes. Their results indicate that it is difficult to solve these tasks by relying purely on superficial image statistics, and can only be solved efficiently through abstract visual reasoning. This makes this setting particularly appealing for investigating the benefits of disentangled representations.

Generating RPM-like Matrices Rather than evaluating disentangled representations on the Procedurally Generated Matrices (PGM) dataset from Barrett et al. [63] we construct two new abstract RPM-like visual reasoning datasets based on two existing datasets for disentangled representation learning. Our motivation for this is twofold: it is not clear what a ground-truth disentangled representation should look like for the PGM dataset, while the two existing disentanglement data sets include the ground-truth factors of variation. Secondly, in using established data sets for disentanglement, we can reuse hyper-parameter ranges that have proven successful. We note that this is substantially different to recent work by Steenbrugge et al. [68] who evaluate the representation of a single trained β -VAE [27] on the original PGM data set.

To construct the abstract reasoning tasks, we use the ground-truth generative model of the *dSprites* [27] and *3dshapes* [42] data sets with the following changes (which we implemented to guarantee that humans can visually distinguish between different values for factors of variation): For *dSprites*, we ignore the orientation feature for the abstract reasoning tasks as certain objects such as squares and ellipses exhibit rotational symmetries. To compensate, we add background color (5 different shades of gray linearly spaced between white and black) and object color (6 different colors linearly spaced in HUSL hue space) as two new factors of variation. Similarly, for the abstract reasoning tasks (but not when training representations), we only consider three different values for the scale of the object (instead of 6) and only four values for the x and y position (instead of 32). For *3dshapes*, we retain all of the original factors but only consider four different values for scale and azimuth (out of 8 and 16) for the abstract reasoning tasks. We refer to Figure 7 in Appendix B for samples from these data sets.

For the modified *dSprites* and *3dshapes*, we now create corresponding abstract reasoning tasks. The key idea is that one is given a 3×3 matrix of context image panels with the bottom right image panel missing, as well as a set of six potential answer panels (see Figure 1 for an example). One then has to infer which of the answers fits in the missing panel of the 3×3 matrix based on relations between image panels in the rows of the 3×3 matrices. Due to the categorical nature of ground-truth factors in the underlying data sets, we focus on the *AND* relationship in which one or more factor values are equal across a sequence of context panels [63].

We generate instances of this abstract reasoning task in the following way: First, we uniformly sample whether 1, 2, or 3 ground-truth factors are fixed across rows in the instance to be generated. Second,

we uniformly sample without replacement the set of underlying factors in the underlying generative model that should be kept constant. Third, we uniformly sample a factor value from the ground-truth model for each of the three rows and for each of the fixed factors.² Fourth, for all other ground-truth factors we also sample 3×3 matrices of factor values from the ground-truth model with the single constraint that the factor values are not allowed to be constant across the first two rows (in that case we sample a new set of values). After this we have ground-truth factor values for each of the 9 panels in the correct solution to the abstract reasoning task, and we can sample corresponding images from the ground-truth model. To generate difficult alternative answers, we take the factor values of the correct answer panel and randomly resample the non-fixed factors as well as a random fixed factor until the factor values no longer satisfy the relations in the original abstract reasoning task. We repeat this process to obtain five incorrect answers and finally insert the correct answers in a random position. Examples of the resulting abstract reasoning tasks can be seen in Figure 1 as well as in Figures 19 and 20 in Appendix C.

Models We will make use of the *Wild Relation Network (WReN)* to solve the abstract visual reasoning tasks [63]. It incorporates relational structure, and was introduced in prior work specifically for such tasks. The *WReN* is evaluated for each answer panel $a \in A = \{a_1, \dots, a_6\}$ in relation to all the context-panels $C = \{c_1, \dots, c_8\}$ as follows:

$$\text{WReN}(a, C) = f_\phi\left(\sum_{e_1, e_2 \in E} g_\theta(e_1, e_2)\right), \quad E = \{\text{CNN}(c_1), \dots, \text{CNN}(c_8)\} \cup \{\text{CNN}(a)\} \quad (2)$$

First an embedding is computed for each panel using a deep Convolutional Neural Network (CNN), which serve as input to a Relation Network (RN) module [64]. The Relation Network reasons about the different relationships between the context and answer panels, and outputs a score. The answer panel $a \in A$ with the highest score is chosen as the final output.

The Relation Network implements a suitable inductive bias for (relational) reasoning [5]. It separates the reasoning process into two stages. First g_θ is applied to all pairs of panel embedding to consider relations between the answer panel and each of the context panels, and relations among the context panels. Weight-sharing of g_θ between the panel-embedding pairs makes it difficult to overfit to the image statistics of the individual panels. Finally, f_ϕ produces a score for the given answer panel in relation to the context panels by globally considering the different relations between the panels as a whole. Note that in using the same *WReN* for different answer panels it is ensured that each answer panel is subject to the same reasoning process.

4 Experiments

4.1 Learning Disentangled Representations

We train β -VAE [27], *FactorVAE* [42], β -TCVAE [10], and *DIP-VAE* [47] on the panels from the modified *dSprites* and *3dshapes* data sets. For β -VAE we consider two variations: the standard version using a fixed β , and a version trained with the *controlled capacity increase* presented by Burgess et al. [9]. Similarly for *DIP-VAE* we consider both the *DIP-VAE-I* and *DIP-VAE-II* variations of the proposed regularizer [47]. For each of these methods, we considered six different values for their (main) hyper-parameter and five different random seeds. The remaining experimental details are presented in Appendix A. We plan to release code to reproduce our results.

After training, we end up with 360 encoders, whose outputs are expected to cover a wide variation of different representational formats with which to encode information in the images. Figures 9 and 10 in the Appendix show histograms of the reconstruction errors obtained after training, and the scores that various disentanglement metrics assigned to the corresponding representations. The reconstructions are mostly good (see also Figure 7), which confirms that the learned representations tend to accurately capture the image content. Correspondingly, we expect any observed difference in up-stream performance when using these representations to be primarily the result of *how* information is encoded. In terms of the scores of the various disentanglement metrics, we observe a wide range of values. It suggests that in going by different definitions of disentanglement, there are large differences among the quality of the learned representations.

²Note that different rows may have different values.

4.2 Abstract Visual Reasoning

We train different WReN models where we control for two potential confounding factors: the representation produced by a specific model used to embed the input images as well as the hyper-parameters of the WReN model. For hyper-parameters, we use a random search space as specified in Appendix A. We used the following training protocol: We train each of these models using a batch size of 32 for 100K iterations where each mini-batch consists of *newly generated* random instances of the abstract reasoning tasks. Similarly, every 1000 iterations, we evaluate the accuracy on 100 mini-batches of fresh samples. We note that this corresponds to the statistical optimization setting, sidestepping the need to investigate the impact of empirical risk minimization and overfitting.³

4.2.1 Initial Study

First, we trained a set of baseline models to assess the overall complexity of the abstract reasoning task. We consider three types of representations: (i) CNN representations which are learned from scratch (with the same architecture as in the disentanglement models) yielding standard WReN, (ii) pre-trained frozen CNN representations based on a random selection of the pre-trained disentanglement models, and (iii) directly using the ground-truth factors of variation (both one-hot encoded and integer encoded). We train 30 different models for each of these approaches and data sets with different random seeds and different draws from the search space over hyper-parameter values.

An overview of the training behaviour and the accuracies achieved can be seen in Figures 2 and 11 (Appendix B). We observe that the standard WReN model struggles to obtain good results on average, even after having seen many different samples at 100K steps. This is due to the fact that training from scratch is hard and runs may get stuck in local minima where they predict each of the answers with equal probabilities. Given the pre-training and the exposure to additional unsupervised samples, it is not surprising that the learned representations from the disentanglement models perform better. The WReN models that are given the true factors also perform well, already after only few steps of training. We also observe that different runs exhibit a significant spread which motivates why we analyze the average accuracy across many runs in the next section.

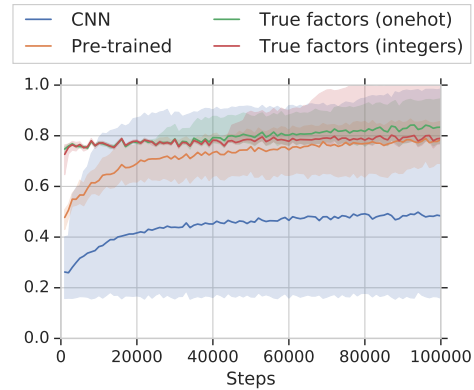


Figure 2: Average up-stream accuracy of baselines, and models using pre-trained representations on *dSprites*. Shaded area indicates min and max accuracy.

It appears that *dSprites* is the harder task, with models reaching an average score of 80%, while reaching an average of 90% on *3dshapes*. Finally, we note that most learning progress takes place in the first 20K steps, and thus expect the benefits of disentangled representations to be most clear in this regime.

4.2.2 Evaluating Disentangled Representations

Based on the results from the initial study, we train a full set of WReN models in the following manner: We first sample a set of 10 hyper-parameter settings from our search space and then trained each of these settings for each of the 360 representations from the disentanglement models. We then compare the average up-stream training accuracy of WReN with the *betaVAE* score, the *factorVAE* score, *MIG*, and the *DCI Disentanglement* score. Additionally we compare the up-stream accuracy with the *reconstruction* error obtained by the decoder on the unsupervised learning task, and with the accuracy of a *Gradient Boosted Tree (GBT10000)* ensemble and a *Logistic Regressor (LR10000)* on single factor classification (averaged across factors) as measured on 10K samples.

Differences in Disentanglement Metrics Figure 3 displays the rank correlation (Spearman) between these metrics and the up-stream classification accuracy, evaluated after training for 1K, 2K,

³Note that the state space of the data generating distribution is very large: 10^6 factor combinations per panel and 14 panels for each instance yield more than 10^{144} potential instances (minus invalid configurations).

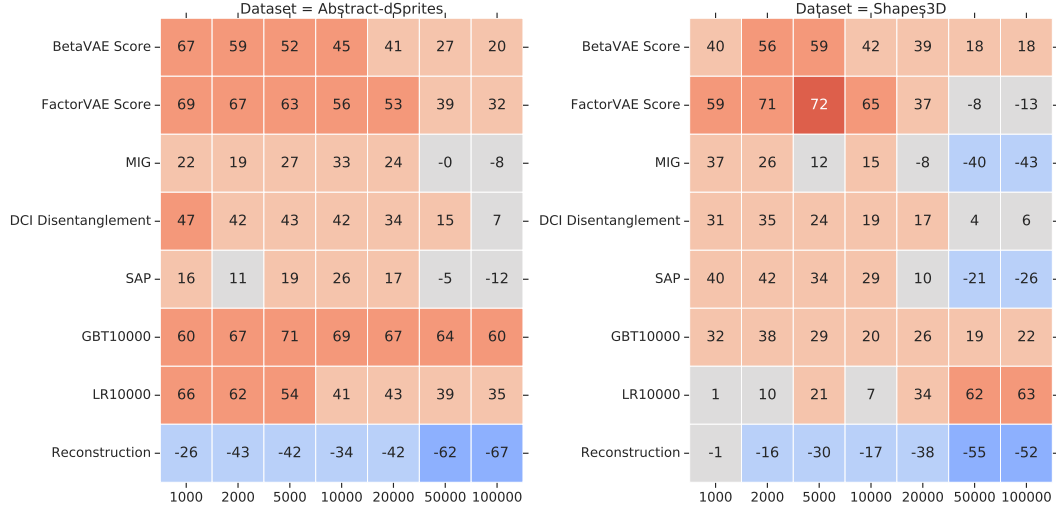


Figure 3: Rank correlation between various metrics and up-stream accuracy of the abstract visual reasoning models throughout training (i.e. for different number of samples).

5K, 10K, 20K, 50K, and 100K steps. If we focus on the disentanglement metrics, several interesting observations can be made. In the few-sample regime (up to 20K steps) and across both data sets it can be seen that both the *betaVAE* score, and the *factorVAE* score are highly correlated with up-stream accuracy. The *DCI disentanglement* score is correlated slightly less, while the *MIG* and *SAP* score exhibit a relatively weak correlation.

These differences between the different disentanglement metrics are perhaps not surprising, as some of these differences are also reflected in their overall correlation (see Figure 3). Note that the *betaVAE* score, and the *factorVAE* score directly measure the effect of intervention, i.e. what happens to the representation if all factors but one are varied, which is expected to be beneficial in efficiently comparing the content of two representations as required for this task. Similarly, it may be that *MIG* and *SAP* score have a more difficult time in differentiating representations that are only partially disentangled. Finally, we note that the best performing metrics on this task are mostly measuring *modularity*, as opposed to *compactness*. A more detailed overview of the correlation between the various metrics and up-stream accuracy can be seen in Figures 12 and 13 in Appendix B.

Disentangled Representations in the Few-Sample Regime If we compare the correlation of the disentanglement metric with the highest correlation (*FactorVAE*) to that of the reconstruction cost in the few-sample regime, then we find that disentanglement correlates much better with up-stream accuracy. Indeed, while low reconstruction error indicates that all information is available in the representation (to reconstruct the image) it makes no assumptions about *how* this information is encoded. We observe strong evidence that disentangled representations yield better up-stream accuracy using relatively few samples, and we therefore conclude that they are indeed more sample efficient compared to entangled representations in this regard.

Figure 4 demonstrates the up-stream accuracy of the WReNs throughout training, binned into quartiles according to their degree of being disentangled as measured by the *FactorVAE* score (left), and in terms of *reconstruction* error (right). It can be seen that representations that are more disentangled give rise to better relative performance consistently throughout all phases of training. If we group models according to their *reconstruction* error then we find that this ordering is much less pronounced. An overview for all other metrics can be seen in Figures 14 and 15.

Disentangled Representations in the Many-Sample Regime In the many-sample regime (i.e. when training for 100K steps on batches of randomly drawn instances in Figure 3) we find that there is no longer a strong correlation to the scores assigned by the various disentanglement metrics and up-stream performance. This is perhaps not surprising as neural networks are general function approximators that, given access to enough labeled samples, are expected to overcome potential difficulties in using entangled representations. The observation that *reconstruction* error correlates much more strongly with up-stream accuracy in this regime further confirms that this is the case.

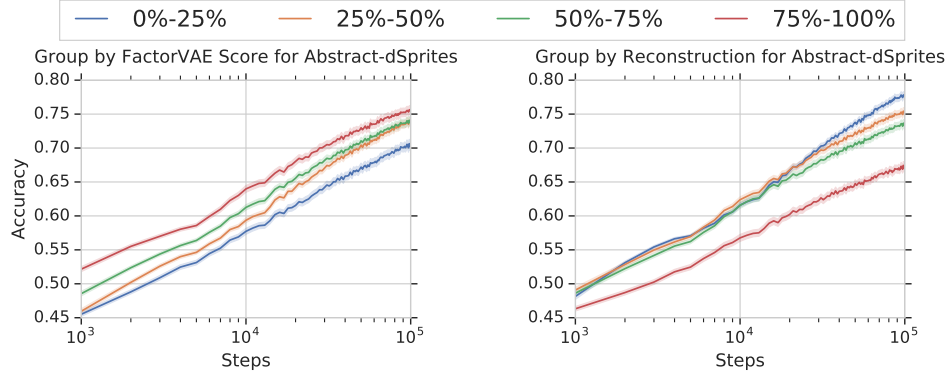


Figure 4: Up-stream accuracy of the abstract visual reasoning models throughout training, binned in quartiles based on the values assigned by the *FactorVAE* score (left), and *reconstruction* error (right)

A similar observation can be made if we look at the difference in up-stream accuracy between the top and bottom half of the models according to each metric in Figures 5 and 16. For all disentanglement metrics, larger positive differences are observed in the few-sample regime that gradually reduce as more samples are observed. Meanwhile, the gap gradually increases for *reconstruction* after seeing additional samples.

Differences in terms of Final Accuracy In our final analysis we consider the rank correlation between up-stream accuracy and the various metrics, split according to their final accuracy. Figure 17 shows the rank correlation for the worst-performing fifty percent of the models after 100K steps (top), and for the best-performing fifty percent (bottom). While these results should be interpreted with care as the split depends on the final accuracy, we still observe interesting results: It can be seen that disentanglement (i.e. *FactorVAE* score) remains strongly correlated with up-stream performance for both splits in the few-sample regime. At the same time, the benefit of lower reconstruction error appears to be limited to the lower 50% of models. The former observation is intuitive as when the reconstruction error is too high, it may be hard to solve the up-stream tasks. However, regarding the best performing models, it appears that the *relative* gains from further reducing reconstruction error are of limited use.

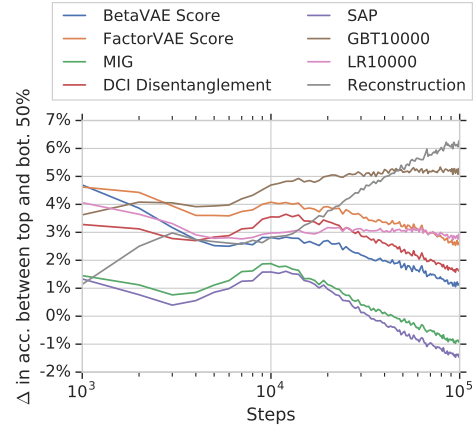


Figure 5: Difference in up-stream accuracy between top 50% and bottom 50%, according to various metrics on *dSprites*.

5 Conclusion

In this work, we investigated whether disentangled representations allow one to learn good models for non-trivial up-stream tasks with fewer samples. We created two abstract visual reasoning tasks based on existing data sets for which the ground truth factors of variation are known. We trained a diverse set of 360 disentanglement models based on four state-of-the-art disentanglement approaches and evaluated their representations using 3600 abstract reasoning models. We observe compelling evidence that more disentangled representations are more sample-efficient in the considered up-stream learning task. We draw three main conclusions from these results: First, these results provide concrete motivation why one might want to pursue disentanglement as a property of learned representations in the unsupervised case. Second, we still observed differences between disentanglement metrics, which we argue should motivate further work in understanding what different properties they capture. We note that none of the metrics achieved perfect correlation in the few-sample regime, which reflects that we have not yet fully understood what makes one representation better than another in terms of learning. Third, it might be useful to extend the methodology in this study to other complex up-stream tasks, or include an investigation of other purported benefits of disentangled representations.

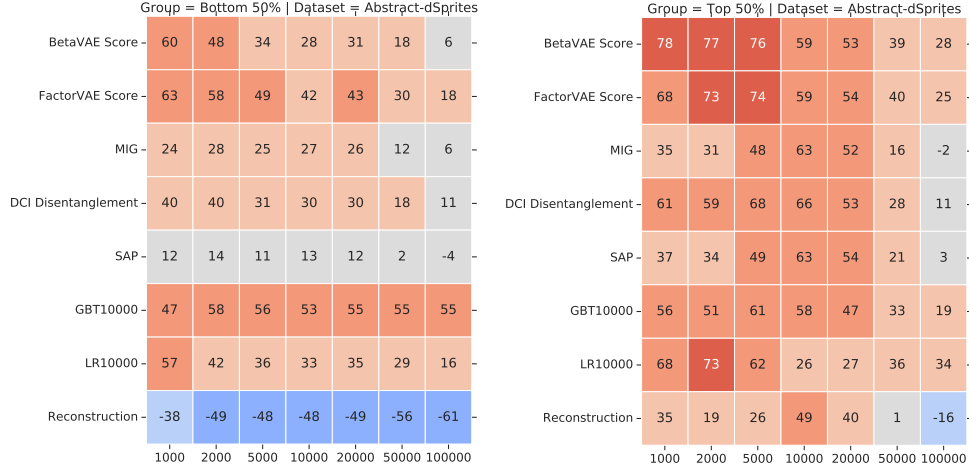


Figure 6: Rank correlation between various metrics and up-stream accuracy of the abstract visual reasoning models throughout training (i.e. for different number of samples). On the left for the worst 50%, and on the right for the best 50% models (based on final up-stream accuracy).

Acknowledgments

The authors thank Adam Santoro, Josip Djolonga, and Paulo Rauber for helpful discussions and comments. This research was partially supported by the Max Planck ETH Center for Learning Systems, an ETH core grant (to Gunnar Rätsch), and the Swiss National Science Foundation (grant 200021_165675/1 to Jürgen Schmidhuber). This work was partially done while Francesco Locatello was at Google Research.

References

- [1] Alessandro Achille, Tom Eccles, Loic Matthey, Chris Burgess, Nicholas Watters, Alexander Lerchner, and Irina Higgins. Life-long disentangled representation learning with cross-domain latent homologies. In *Advances in Neural Information Processing Systems*, pages 9873–9883, 2018.
- [2] Francis Bach and Michael Jordan. Kernel independent component analysis. *Journal of Machine Learning Research*, 3(7):1–48, 2002.
- [3] H. B. Barlow. Unsupervised learning. *Neural Computation*, 1(3):295–311, 1989.
- [4] H. B. Barlow, T. P. Kaushal, and G. J. Mitchison. Finding minimum entropy codes. *Neural Computation*, 1(3):412–423, 1989.
- [5] Peter W Battaglia, Jessica B Hamrick, Victor Bapst, Alvaro Sanchez-Gonzalez, Vinicius Zambaldi, Mateusz Malinowski, Andrea Tacchetti, David Raposo, Adam Santoro, Ryan Faulkner, et al. Relational inductive biases, deep learning, and graph networks. *arXiv preprint arXiv:1806.01261*, 2018.
- [6] Yoshua Bengio, Aaron Courville, and Pascal Vincent. Representation learning: A review and new perspectives. *IEEE transactions on pattern analysis and machine intelligence*, 35(8):1798–1828, 2013.
- [7] Yoshua Bengio, Yann LeCun, et al. Scaling learning algorithms towards AI. *Large-scale Kernel Machines*, 34(5):1–41, 2007.
- [8] Diane Bouchacourt, Ryota Tomioka, and Sebastian Nowozin. Multi-level variational autoencoder: Learning disentangled representations from grouped observations. In *AAAI Conference on Artificial Intelligence*, 2018.
- [9] Christopher P Burgess, Irina Higgins, Arka Pal, Loic Matthey, Nick Watters, Guillaume Desjardins, and Alexander Lerchner. Understanding disentangling in β -vae. *NIPS Workshop on Learning Disentangled Representations: From Perception to Control*, 2017.

- [10] Ricky TQ Chen, Xuechen Li, Roger Grosse, and David Duvenaud. Isolating sources of disentanglement in vaes. In *Proceedings of the 32nd International Conference on Neural Information Processing Systems*, pages 2615–2625. Curran Associates Inc., 2018.
- [11] Brian Cheung, Jesse A Livezey, Arjun K Bansal, and Bruno A Olshausen. Discovering hidden factors of variation in deep networks. *arXiv preprint arXiv:1412.6583*, 2014.
- [12] Taco Cohen and Max Welling. Learning the irreducible representations of commutative lie groups. In *International Conference on Machine Learning*, 2014.
- [13] Pierre Comon. Independent component analysis, a new concept? *Signal Processing*, 36(3):287–314, 1994.
- [14] Zhiwei Deng, Rajitha Navarathna, Peter Carr, Stephan Mandt, Yisong Yue, Iain Matthews, and Greg Mori. Factorized variational autoencoders for modeling audience reactions to movies. In *IEEE Conference on Computer Vision and Pattern Recognition*, 2017.
- [15] Emily L Denton and Vighnesh Birodkar. Unsupervised learning of disentangled representations from video. In *Advances in Neural Information Processing Systems*, 2017.
- [16] Cian Eastwood and Christopher K. I. Williams. A framework for the quantitative evaluation of disentangled representations. In *International Conference on Learning Representations*, 2018.
- [17] SM Ali Eslami, Nicolas Heess, Theophane Weber, Yuval Tassa, David Szepesvari, Geoffrey E Hinton, et al. Attend, infer, repeat: Fast scene understanding with generative models. In *Advances in Neural Information Processing Systems*, pages 3225–3233, 2016.
- [18] Babak Esmaeili, Hao Wu, Sarthak Jain, Alican Bozkurt, N Siddharth, Brooks Paige, Dana H Brooks, Jennifer Dy, and Jan-Willem Meent. Structured disentangled representations. In *The 22nd International Conference on Artificial Intelligence and Statistics*, pages 2525–2534, 2019.
- [19] Vincent Fortuin, Matthias Hüser, Francesco Locatello, Heiko Strathmann, and Gunnar Rätsch. Deep self-organization: Interpretable discrete representation learning on time series. In *International Conference on Learning Representations*, 2019.
- [20] Marco Fraccaro, Simon Kamronn, Ulrich Paquet, and Ole Winther. A disentangled recognition and nonlinear dynamics model for unsupervised learning. In *Advances in Neural Information Processing Systems*, 2017.
- [21] Ross Goroshin, Michael F Mathieu, and Yann LeCun. Learning to linearize under uncertainty. In *Advances in Neural Information Processing Systems*, 2015.
- [22] Klaus Greff, Raphaël Lopez Kaufmann, Rishab Kabra, Nick Watters, Chris Burgess, Daniel Zoran, Loic Matthey, Matthew Botvinick, and Alexander Lerchner. Multi-object representation learning with iterative variational inference. In *Proceedings of the 36th International Conference on Machine Learning-Volume 97*, 2019.
- [23] Klaus Greff, Antti Rasmus, Mathias Berglund, Tele Hao, Harri Valpola, and Jürgen Schmidhuber. Tagger: Deep unsupervised perceptual grouping. In *Advances in Neural Information Processing Systems*, pages 4484–4492, 2016.
- [24] Klaus Greff, Sjoerd van Steenkiste, and Jürgen Schmidhuber. Neural expectation maximization. In *Advances in Neural Information Processing Systems*, pages 6691–6701, 2017.
- [25] Luigi Gresele, Paul K. Rubenstein, Arash Mehrjou, Francesco Locatello, and Bernhard Schölkopf. The incomplete rosetta stone problem: Identifiability results for multi-view nonlinear ica. In *Conference on Uncertainty in Artificial Intelligence (UAI)*, 2019.
- [26] Irina Higgins, David Amos, David Pfau, Sebastien Racaniere, Loic Matthey, Danilo Rezende, and Alexander Lerchner. Towards a definition of disentangled representations. *arXiv preprint arXiv:1812.02230*, 2018.
- [27] Irina Higgins, Loic Matthey, Arka Pal, Christopher Burgess, Xavier Glorot, Matthew Botvinick, Shakir Mohamed, and Alexander Lerchner. beta-vae: Learning basic visual concepts with a constrained variational framework. In *International Conference on Learning Representations*, volume 3, 2017.
- [28] Irina Higgins, Arka Pal, Andrei Rusu, Loic Matthey, Christopher Burgess, Alexander Pritzel, Matthew Botvinick, Charles Blundell, and Alexander Lerchner. Darla: Improving zero-shot transfer in reinforcement learning. In *Proceedings of the 34th International Conference on Machine Learning-Volume 70*, pages 1480–1490. JMLR. org, 2017.

- [29] Irina Higgins, Nicolas Sonnerat, Loic Matthey, Arka Pal, Christopher P Burgess, Matko Bošnjak, Murray Shanahan, Matthew Botvinick, Demis Hassabis, and Alexander Lerchner. SCAN: Learning hierarchical compositional visual concepts. In *International Conference on Learning Representations*, 2018.
- [30] Felix Hill, Adam Santoro, David Barrett, Ari Morcos, and Timothy Lillicrap. Learning to make analogies by contrasting abstract relational structure. In *International Conference on Learning Representations*, 2019.
- [31] Geoffrey E Hinton, Alex Krizhevsky, and Sida D Wang. Transforming auto-encoders. In *International Conference on Artificial Neural Networks*, 2011.
- [32] S. Hochreiter and J. Schmidhuber. Feature extraction through LOCOCODE. *Neural Computation*, 11(3):679–714, 1999.
- [33] S. Hochreiter and J. Schmidhuber. Nonlinear ICA through low-complexity autoencoders. In *Proceedings of the 1999 IEEE International Symposium on Circuits and Systems (ISCAS’99)*, volume 5, pages 53–56. IEEE, 1999.
- [34] Jun-Ting Hsieh, Bingbin Liu, De-An Huang, Li F Fei-Fei, and Juan Carlos Nieves. Learning to decompose and disentangle representations for video prediction. In *Advances in Neural Information Processing Systems*, 2018.
- [35] Wei-Ning Hsu, Yu Zhang, and James Glass. Unsupervised learning of disentangled and interpretable representations from sequential data. In *Advances in neural information processing systems*, pages 1878–1889, 2017.
- [36] Aapo Hyvarinen and Hiroshi Morioka. Unsupervised feature extraction by time-contrastive learning and nonlinear ica. In *Advances in Neural Information Processing Systems*, 2016.
- [37] Aapo Hyvärinen and Petteri Pajunen. Nonlinear independent component analysis: Existence and uniqueness results. *Neural Networks*, 1999.
- [38] Aapo Hyvarinen, Hiroaki Sasaki, and Richard E Turner. Nonlinear ica using auxiliary variables and generalized contrastive learning. In *International Conference on Artificial Intelligence and Statistics*, 2019.
- [39] Christian Jutten and Juha Karhunen. Advances in nonlinear blind source separation. In *International Symposium on Independent Component Analysis and Blind Signal Separation*, pages 245–256, 2003.
- [40] Theofanis Karaletsos, Serge Belongie, and Gunnar Rätsch. Bayesian representation learning with oracle constraints. In *International Conference on Learning Representations*, 2016.
- [41] Charles Kemp and Joshua B Tenenbaum. The discovery of structural form. *Proceedings of the National Academy of Sciences*, 105(31):10687–10692, 2008.
- [42] Hyunjik Kim and Andriy Mnih. Disentangling by factorising. In *International Conference on Machine Learning*, pages 2654–2663, 2018.
- [43] Diederik P Kingma, Shakir Mohamed, Danilo Jimenez Rezende, and Max Welling. Semi-supervised learning with deep generative models. In *Advances in Neural Information Processing Systems*, 2014.
- [44] Diederik P Kingma and Max Welling. Auto-encoding variational bayes. In *International Conference on Learning Representations*, 2014.
- [45] Jack Klys, Jake Snell, and Richard Zemel. Learning latent subspaces in variational autoencoders. In *Advances in Neural Information Processing Systems*, 2018.
- [46] Tejas D Kulkarni, William F Whitney, Pushmeet Kohli, and Josh Tenenbaum. Deep convolutional inverse graphics network. In *Advances in Neural Information Processing Systems*, 2015.
- [47] Abhishek Kumar, Prasanna Sattigeri, and Avinash Balakrishnan. VARIATIONAL INFERENCE OF DISENTANGLED LATENT CONCEPTS FROM UNLABELED OBSERVATIONS. In *International Conference on Learning Representations*, 2018.
- [48] Brenden M Lake, Tomer D Ullman, Joshua B Tenenbaum, and Samuel J Gershman. Building machines that learn and think like people. *Behavioral and brain sciences*, 40, 2017.
- [49] Yann LeCun, Yoshua Bengio, and Geoffrey Hinton. Deep learning. *Nature*, 521(7553):436, 2015.

- [50] Francesco Locatello, Stefan Bauer, Mario Lucic, Sylvain Gelly, Bernhard Schölkopf, and Olivier Bachem. Challenging common assumptions in the unsupervised learning of disentangled representations. In *Proceedings of the 36th International Conference on Machine Learning-Volume 97*, 2018.
- [51] Francesco Locatello, Michael Tschannen, Stefan Bauer, Gunnar Rätsch, Bernhard Schölkopf, and Olivier Bachem. Disentangling factors of variation using few labels. *arXiv preprint arXiv:1905.01258*, 2019.
- [52] Francesco Locatello, Damien Vincent, Ilya Tolstikhin, Gunnar Rätsch, Sylvain Gelly, and Bernhard Schölkopf. Competitive training of mixtures of independent deep generative models. In *Workshop at the 6th International Conference on Learning Representations (ICLR)*, 2018.
- [53] Romain Lopez, Jeffrey Regier, Michael I Jordan, and Nir Yosef. Information constraints on auto-encoding variational bayes. In *Advances in Neural Information Processing Systems*, pages 6114–6125, 2018.
- [54] William Lotter, Gabriel Kreiman, and David Cox. Deep predictive coding networks for video prediction and unsupervised learning. In *International Conference on Learning Representations*, 2017.
- [55] Michael F Mathieu, Junbo J Zhao, Aditya Ramesh, Pablo Sprechmann, and Yann LeCun. Disentangling factors of variation in deep representation using adversarial training. In *Advances in Neural Information Processing Systems*, 2016.
- [56] Siddharth Narayanaswamy, T Brooks Paige, Jan-Willem Van de Meent, Alban Desmaison, Noah Goodman, Pushmeet Kohli, Frank Wood, and Philip Torr. Learning disentangled representations with semi-supervised deep generative models. In *Advances in Neural Information Processing Systems*, 2017.
- [57] Jonas Peters, Dominik Janzing, and Bernhard Schölkopf. *Elements of Causal Inference - Foundations and Learning Algorithms*. Adaptive Computation and Machine Learning Series. MIT Press, 2017.
- [58] D Raposo, A Santoro, DGT Barrett, R Pascanu, T Lillicrap, and P Battaglia. Discovering objects and their relations from entangled scene representations. *International Conference on Learning Representations, Workshop Track*, 2017.
- [59] John C Raven. Standardization of progressive matrices, 1938. *British Journal of Medical Psychology*, 19(1):137–150, 1941.
- [60] Scott Reed, Kihyuk Sohn, Yuting Zhang, and Honglak Lee. Learning to disentangle factors of variation with manifold interaction. In *International Conference on Machine Learning*, 2014.
- [61] Karl Ridgeway and Michael C Mozer. Learning deep disentangled embeddings with the f-statistic loss. In *Advances in Neural Information Processing Systems*, pages 185–194, 2018.
- [62] Adrià Ruiz, Oriol Martinez, Xavier Binefa, and Jakob Verbeek. Learning disentangled representations with reference-based variational autoencoders. *arXiv preprint arXiv:1901.08534*, 2019.
- [63] Adam Santoro, Felix Hill, David Barrett, Ari Morcos, and Timothy Lillicrap. Measuring abstract reasoning in neural networks. In *International Conference on Machine Learning*, pages 4477–4486, 2018.
- [64] Adam Santoro, David Raposo, David G Barrett, Mateusz Malinowski, Razvan Pascanu, Peter Battaglia, and Timothy Lillicrap. A simple neural network module for relational reasoning. In *Advances in neural information processing systems*, pages 4967–4976, 2017.
- [65] J. Schmidhuber. "deep learning in neural networks: An overview. *Neural Networks*, 61:85–117, 2015. Published online 2014; 888 references; based on TR arXiv:1404.7828 [cs.NE].
- [66] J. Schmidhuber, M. Eldracher, and B. Foltin. Semilinear predictability minimization produces well-known feature detectors. *Neural Computation*, 8(4):773–786, 1996.
- [67] Jürgen Schmidhuber. Learning factorial codes by predictability minimization. *Neural Computation*, 4(6):863–879, 1992.
- [68] Xander Steenbrugge, Sam Leroux, Tim Verbelen, and Bart Dhoedt. Improving generalization for abstract reasoning tasks using disentangled feature representations. *Neural Information Processing Systems (NeurIPS) 2018 Workshop on Relational Representation Learning, Montréal, Canada.*, 2018.

- [69] Raphael Suter, Djordje Miladinović, Stefan Bauer, and Bernhard Schölkopf. Interventional robustness of deep latent variable models. In *(To appear) International Conference on Machine Learning*, 2019.
- [70] Joshua B Tenenbaum and William T Freeman. Separating style and content with bilinear models. *Neural computation*, 12(6):1247–1283, 2000.
- [71] Michael Tschannen, Olivier Bachem, and Mario Lucic. Recent advances in autoencoder-based representation learning. *Third workshop on Bayesian Deep Learning (NeurIPS 2018), Montreal, Canada.*, 2018.
- [72] Sjoerd van Steenkiste, Michael Chang, Klaus Greff, and Jürgen Schmidhuber. Relational neural expectation maximization: Unsupervised discovery of objects and their interactions. In *International Conference on Learning Representations*, 2018.
- [73] Pascal Vincent, Hugo Larochelle, Yoshua Bengio, and Pierre-Antoine Manzagol. Extracting and composing robust features with denoising autoencoders. In *Proceedings of the 25th international conference on Machine learning*, pages 1096–1103. ACM, 2008.
- [74] Satoshi Watanabe. Information theoretical analysis of multivariate correlation. *IBM Journal of research and development*, 4(1):66–82, 1960.
- [75] William F Whitney, Michael Chang, Tejas Kulkarni, and Joshua B Tenenbaum. Understanding visual concepts with continuation learning. *International Conference on Learning Representations, Workshop Track*, 2016.
- [76] Jimei Yang, Scott E Reed, Ming-Hsuan Yang, and Honglak Lee. Weakly-supervised disentangling with recurrent transformations for 3D view synthesis. In *Advances in Neural Information Processing Systems*, 2015.
- [77] Li Yingzhen and Stephan Mandt. Disentangled sequential autoencoder. In *International Conference on Machine Learning*, 2018.

A Architectures and Hyper-parameters

A.1 Disentanglement Methods

We use the same architecture, hyper-parameters and training setup as in [50], which we report here for completeness. The architecture is depicted in Table 1. All models share the following hyper-parameters: We used a batch size of 64, 10-dimensional latent space and Bernoulli decoders. We trained the models for 300K steps using the Adam optimizer with $\beta_1 = 0.9$, $\beta_2 = 0.999$, $\epsilon = 10^{-8}$ and a learning rate of 0.0001.

For β -VAE, we perform a sweep on β on the interval $[1, 2, 4, 6, 8, 16]$. For β -VAE with *controlled capacity increase*, we perform a sweep on c_{max} on the interval $[5, 10, 25, 50, 75, 100]$. The iteration threshold is set to 100K and $\gamma = 1000$. For *FactorVAE*, we perform a sweep on γ on the interval $[10, 20, 30, 40, 50, 100]$. For the discriminator of the *FactorVAE* we use the architecture described in Table 2. The hyper-parameters for the discriminator are: Batch size = 64, Optimizer = Adam, Adam: beta1 = 0.5, Adam: beta2 = 0.9, Adam: epsilon = 1e-8, Adam: learning rate = 0.0001. For *DIP-VAE-I*, we perform a sweep on λ_{od} on the interval $[1, 2, 5, 10, 20, 50]$. We further set $\lambda_d = 10$. For *DIP-VAE-II*, we perform a sweep on β on the interval $[1, 2, 5, 10, 20, 50]$. We further set $\lambda_d = 10$. For β -TCVAE, we perform a sweep on β on the interval $[1, 2, 4, 6, 8, 10]$. Each model is trained using 5 different random seeds.

Table 1: Encoder and Decoder architectures.

| Encoder | Decoder |
|--|---|
| Input: $64 \times 64 \times \text{number of channels}$ | Input: \mathbb{R}^{10} |
| 4×4 conv, 32 ReLU, stride 2 | FC, 256 ReLU |
| 4×4 conv, 32 ReLU, stride 2 | FC, $4 \times 4 \times 64$ ReLU |
| 4×4 conv, 64 ReLU, stride 2 | 4×4 upconv, 64 ReLU, stride 2 |
| 4×4 conv, 64 ReLU, stride 2 | 4×4 upconv, 32 ReLU, stride 2 |
| FC 256, FC 2×10 | 4×4 upconv, 32 ReLU, stride 2 |
| | 4×4 upconv, number of channels, stride 2 |

Table 2: Architecture for the discriminator in *FactorVAE*.

| Discriminator |
|---------------------|
| FC, 1000 leaky ReLU |
| FC, 1000 leaky ReLU |
| FC, 1000 leaky ReLU |
| FC, 1000 leaky ReLU |
| FC, 1000 leaky ReLU |
| FC, 1000 leaky ReLU |
| FC, 2 |

A.2 Abstract Visual Reasoning Method

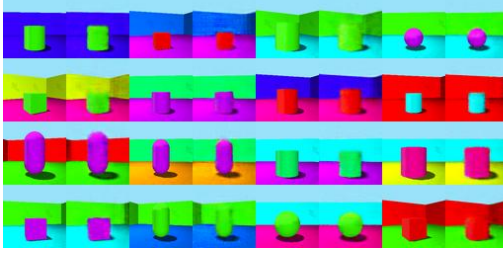
To solve the abstract reasoning tasks, we implemented the *Wild Relation Networks (WReN)* model of Barrett et al. [63]. For the experiments, we use the following random search space over the hyper-parameters: We uniformly sample a learning rate for the Adam optimizer from the set $\{0.01, 0.001, 0.0001\}$ while β_1 is set to 0.9, β_2 to 0.999, and ϵ to 10^{-8} . For the edge MLP g in the *WReN* model, we uniformly choose either 256 or 512 hidden units and we uniformly sample whether it has 2, 3, or 4 hidden layers. Similarly, for the graph MLP f in the *WReN* model, we uniformly choose either 128 or 256 hidden units and we uniformly sample whether it has 1 or 2 hidden layers before the final linear layer to compute the final score. We also uniformly sample whether we apply no dropout, dropout of 0.25, dropout of 0.5, or dropout of 0.75 to units before this last layer.

B Additional Results

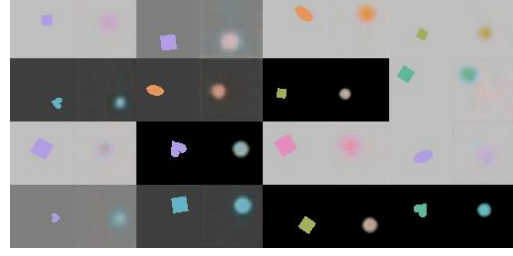
B.1 Additional Results of Representation Learning

This subsection contains additional results in evaluating the training of the 360 disentanglement models. Figure 7 presents example reconstructions for different data sets and models that are representative of the median reconstruction error. Figure 8 displays the rank correlation between the various metrics on the learned representations, and

Finally, Figures 9 and 10 present histograms of the scores assigned by various metrics to the learned representations on *dSprites* and *shapes3d* respectively.



(a) DIP-VAE-I trained on Shapes3D.



(b) FactorVAE trained on Abstract-dSprites.

Figure 7: Reconstructions for different data sets and models (representative samples of median reconstruction error). Odd columns show real samples and even columns their reconstruction. Shapes3D appears to be much easier than Abstract-dSprites where disentangling the shape appears hard.

| Dataset = Abstract-dSprites | | | | | | | | | Dataset = Shapes3D | | | | | | | | |
|-----------------------------|-----|-----|-----|-----|-----|-----|-----|-----|---------------------|-----|-----|-----|-----|-----|-----|-----|-----|
| BetaVAE Score | 100 | 85 | 42 | 70 | 40 | 50 | 71 | 10 | BetaVAE Score | 100 | 75 | 18 | 52 | 49 | 59 | 36 | -27 |
| FactorVAE Score | 85 | 100 | 46 | 69 | 46 | 56 | 64 | -2 | FactorVAE Score | 75 | 100 | 37 | 43 | 63 | 43 | 2 | -2 |
| MIG | 42 | 46 | 100 | 77 | 89 | 47 | 2 | 40 | MIG | 18 | 37 | 100 | 66 | 68 | 49 | -58 | 64 |
| DCI Disentanglement | 70 | 69 | 77 | 100 | 73 | 68 | 33 | 25 | DCI Disentanglement | 52 | 43 | 66 | 100 | 54 | 95 | -10 | 25 |
| SAP | 40 | 46 | 89 | 73 | 100 | 36 | 5 | 48 | SAP | 49 | 63 | 68 | 54 | 100 | 46 | -26 | 33 |
| GBT10000 | 50 | 56 | 47 | 68 | 36 | 100 | 31 | -27 | GBT10000 | 59 | 43 | 49 | 95 | 46 | 100 | 10 | 5 |
| LR10000 | 71 | 64 | 2 | 33 | 5 | 31 | 100 | -16 | LR10000 | 36 | 2 | -58 | -10 | -26 | 10 | 100 | -77 |
| Reconstruction | 10 | -2 | 40 | 25 | 48 | -27 | -16 | 100 | Reconstruction | -27 | -2 | 64 | 25 | 33 | 5 | -77 | 100 |
| BetaVAE Score | | | | | | | | | BetaVAE Score | | | | | | | | |
| FactorVAE Score | | | | | | | | | FactorVAE Score | | | | | | | | |
| MIG | | | | | | | | | MIG | | | | | | | | |
| DCI Disentanglement | | | | | | | | | DCI Disentanglement | | | | | | | | |
| SAP | | | | | | | | | SAP | | | | | | | | |
| GBT10000 | | | | | | | | | GBT10000 | | | | | | | | |
| LR10000 | | | | | | | | | LR10000 | | | | | | | | |
| Reconstruction | | | | | | | | | Reconstruction | | | | | | | | |

Figure 8: Rank correlations between the different metrics considered in this paper.

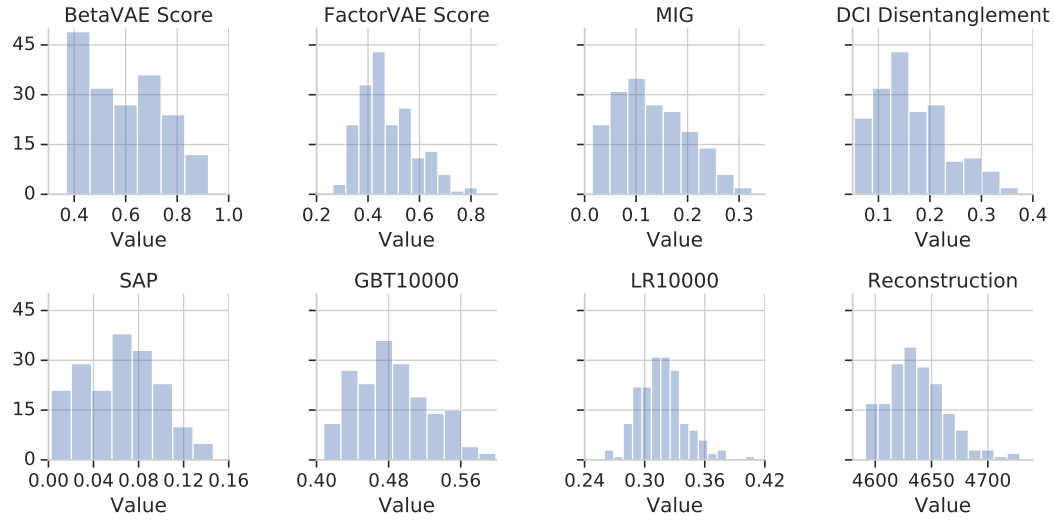


Figure 9: Distribution of scores assigned by various metrics to the learned representations on *dSprites*.

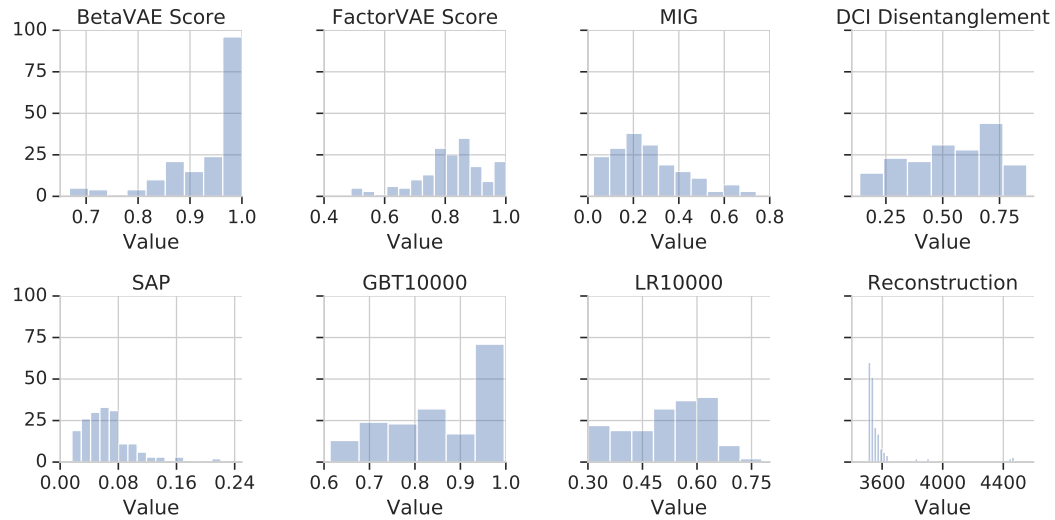


Figure 10: Distribution of scores assigned by various metrics to the learned representations on *3dshapes*.

B.2 Additional Results of Abstract Visual Reasoning

This subsection contains additional results obtained after training 3600 WReN models on the up-stream abstract visual reasoning tasks. Figure 11 presents the results for the various baselines on *3dshapes*. Figures 12 and 13 provide an in-depth view of the correlation between the scores assigned by various metrics and the up-stream accuracy.

Figures 14 and 15 present the up-stream accuracy at various stages of training of models grouped in quartiles according to the scores assigned by a given metric on *dSprites* and *3dshapes* respectively. Figure 16 presents the difference in up-stream accuracy of the best 50% and worst 50% as determined by each metric throughout training on *3dshapes*.

Finally, Figure 17 presents the rank correlation between the scores of various metrics and up-stream accuracy for the upper- and lower 50% of the models as determined by their up-stream accuracy after training for 100K steps.

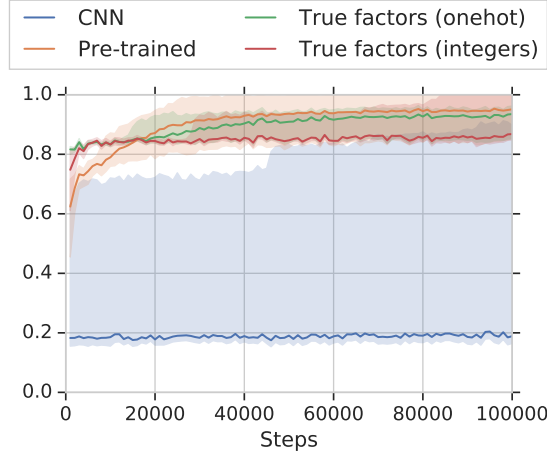


Figure 11: Up-stream accuracy of baselines, and models using pre-trained representations on *3dshapes*. Shaded area indicates min / max.

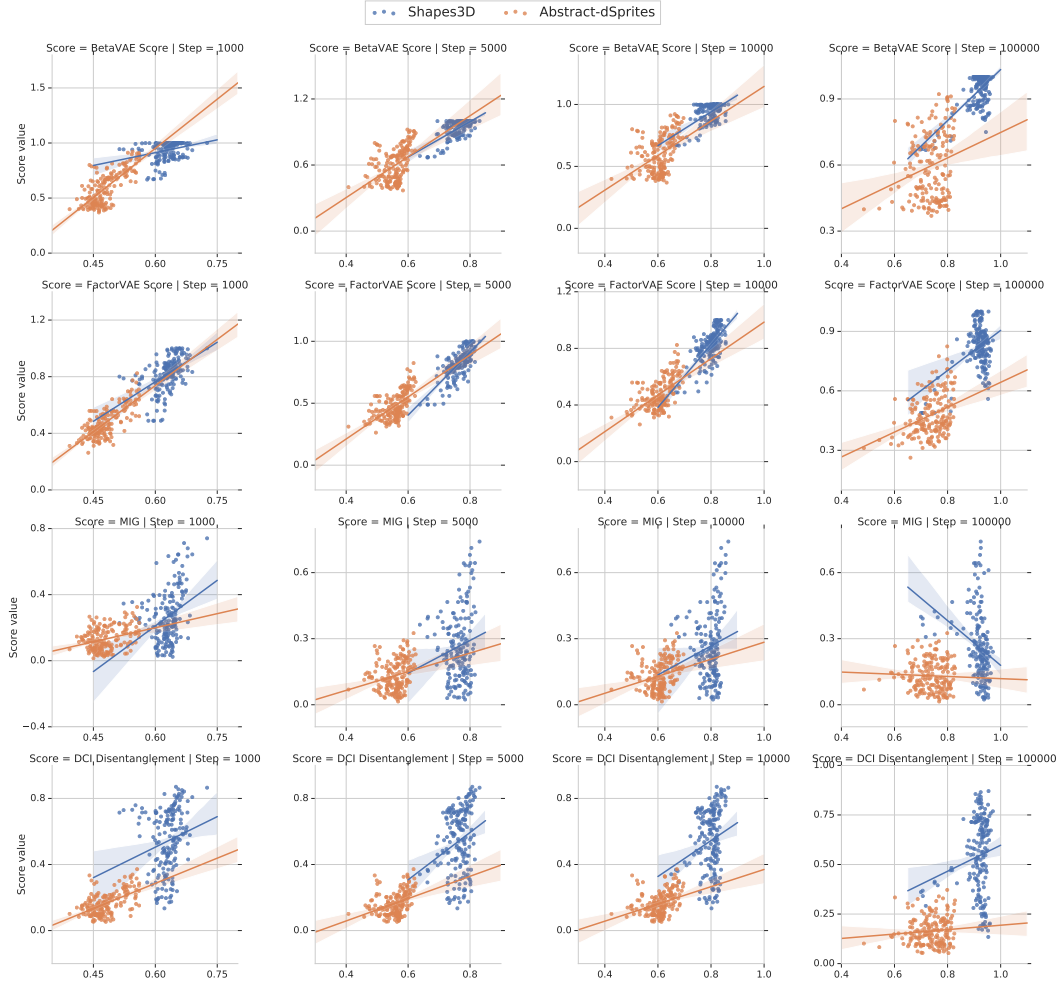


Figure 12: Correlation between *BetaVAE* score, *FactorVAE* score, *MIG*, and *DCI Disentanglement* score (rows) and up-stream accuracy of the abstract visual reasoning models. Columns correspond to 1K, 5K, 10K, 100K training steps (i.e. number of samples).

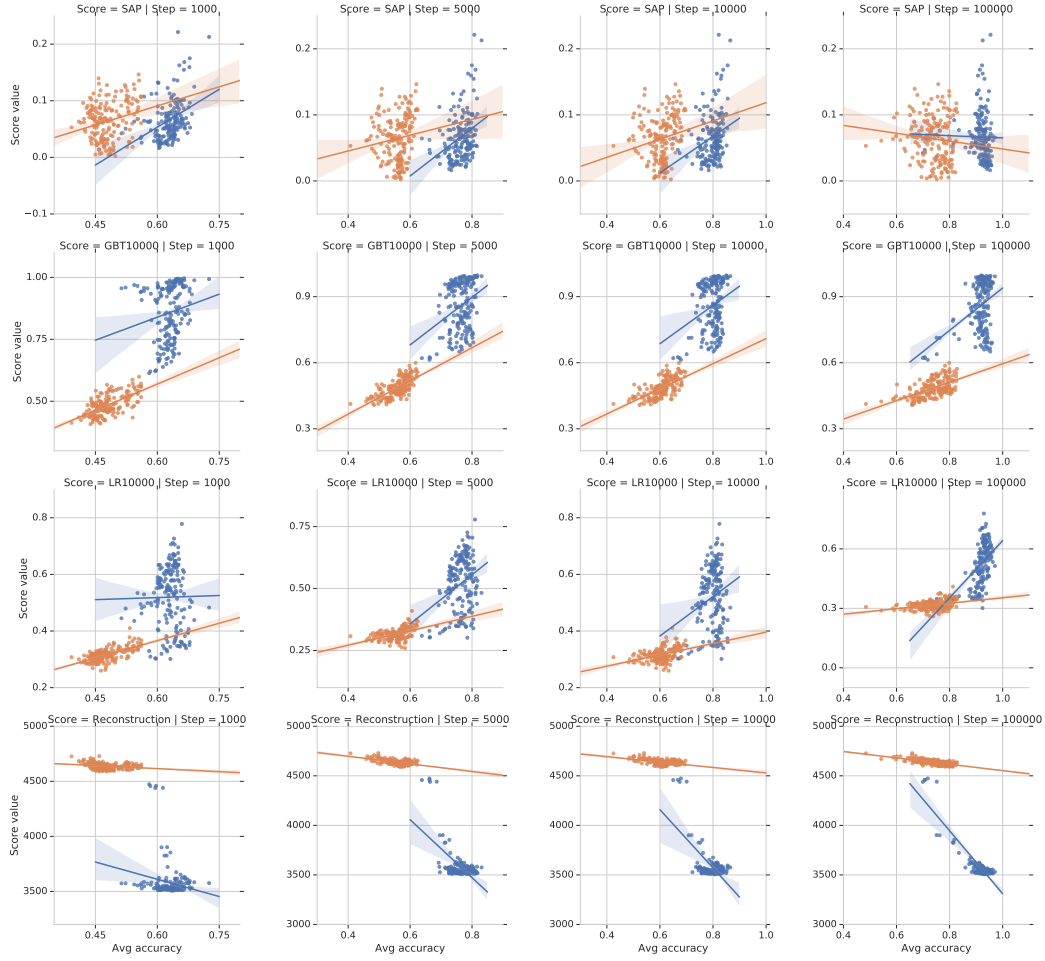


Figure 13: Correlation between *SAP* score, *GBT10000*, *LR10000*, and *reconstruction* error (rows) and up-stream accuracy of the abstract visual reasoning models. Columns correspond to 1K, 5K, 10K, 100K training steps (i.e. number of samples).

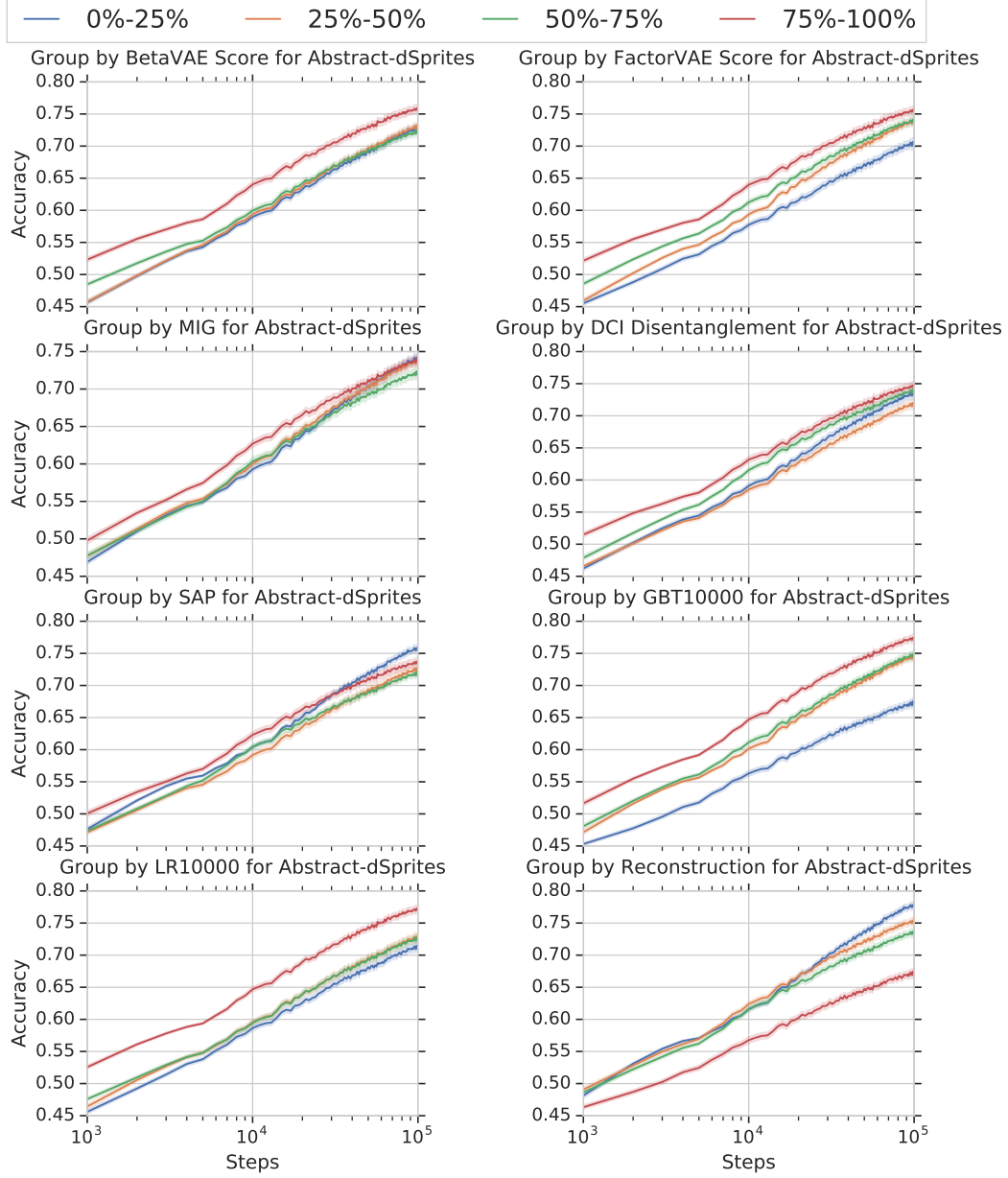


Figure 14: Up-stream accuracy of abstract visual reasoning models on *dSprites* throughout training (i.e. for different number of samples) binned in quartiles based on different metrics

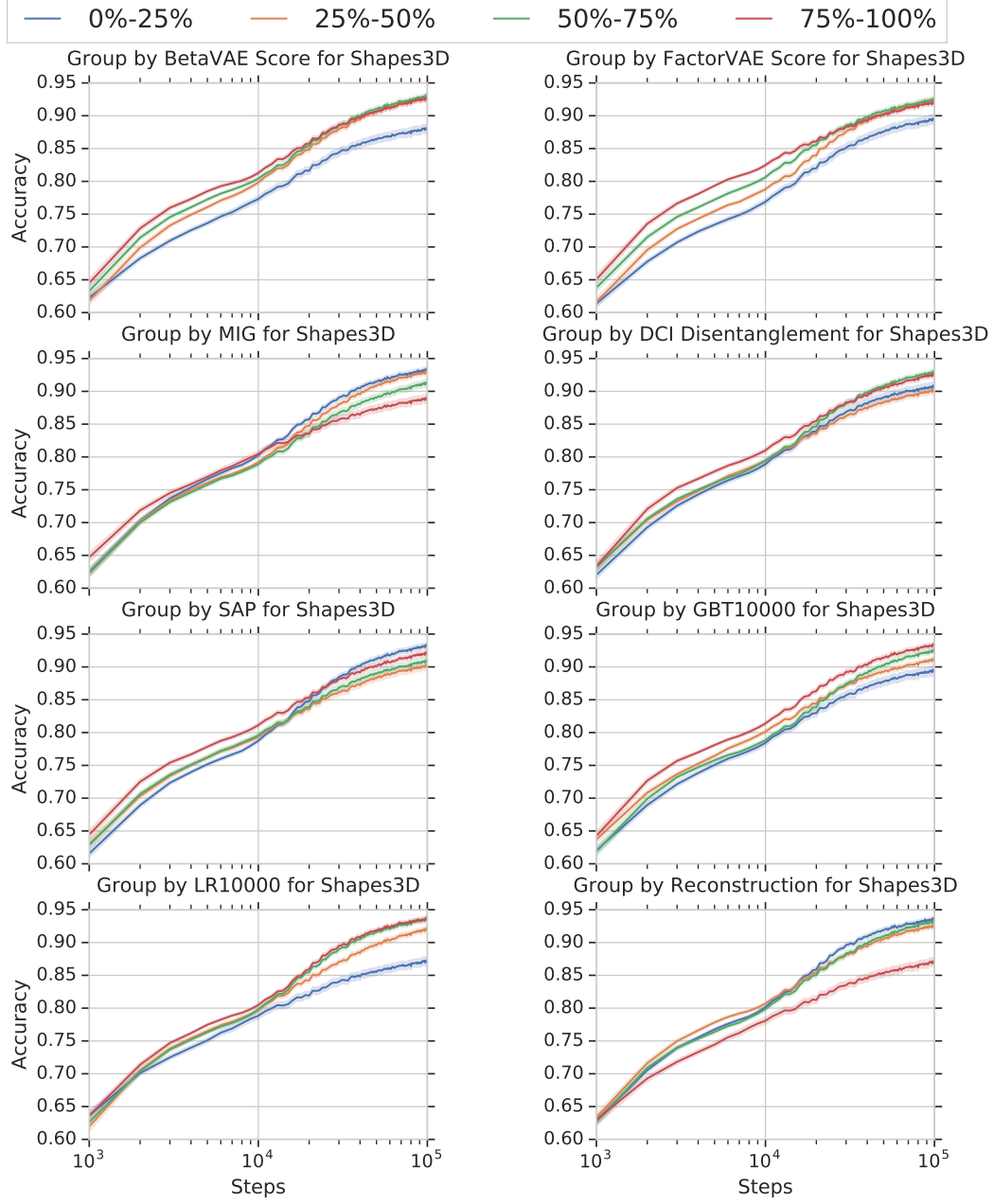


Figure 15: Up-stream accuracy of abstract visual reasoning models on *3dshapes* throughout training (i.e. for different number of samples) binned in quartiles based on different metrics

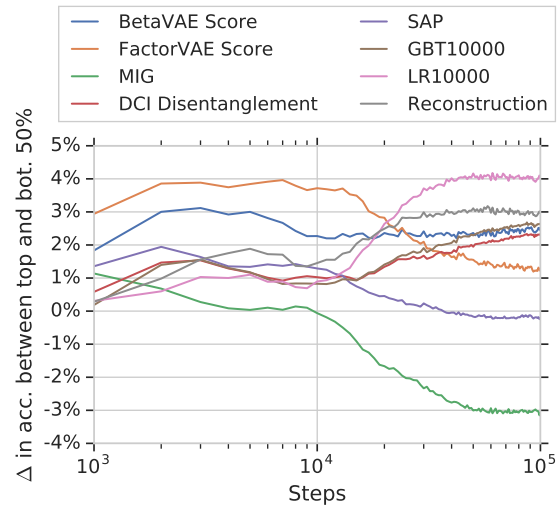


Figure 16: Difference in up-stream accuracy between top 50% and bottom 50%, according to various metrics on *3dshapes*. X-axis is in log scale.

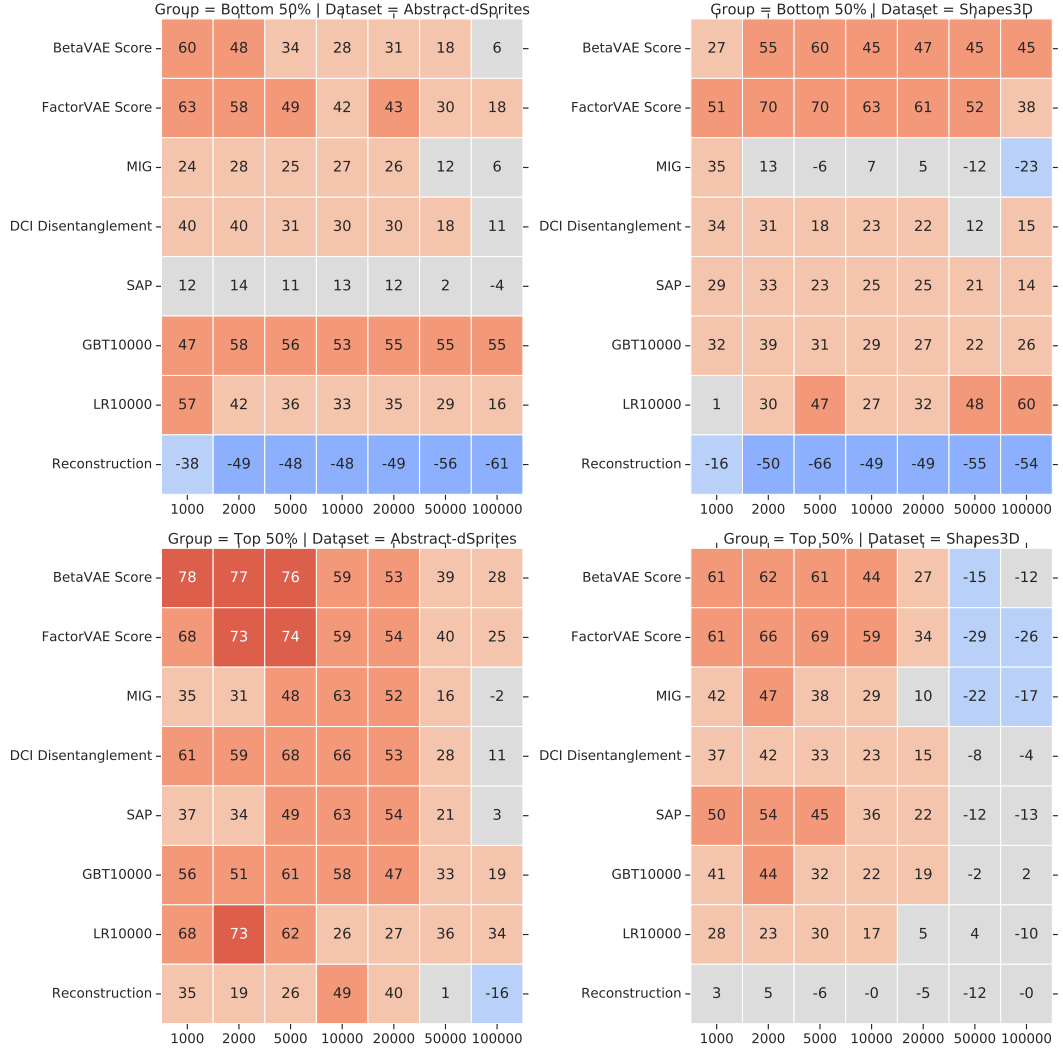


Figure 17: Rank correlation between various metrics and up-stream accuracy of the abstract visual reasoning models throughout training (i.e. for different number of samples). Top row correspond to worst 50% of the models (based on final accuracy), and bottom row corresponds to best 50% of the models. Columns correspond to different data sets.

C Abstract Visual Reasoning Data

Figure 18 contains the answers to the PGM-like abstract visual reasoning tasks on *dSprites* and *shapes3d*. Focusing on the right example in Figure 18, note that the correct answer cannot be found by only considering the incomplete sequence of the context panel and the answer panels. In particular, we can not tell whether 1, 2 or 3 relationships hold and if for example the wall color or the object color is constant. As a result, one must consider the other two rows of context panels to deduce that it is background color, the azimuth and the shape-type that are equal among the panels. Then, this insight needs to be applied to the bottom row to see that a cylinder, a specific view point, and a lighter blue background are required in the correct solution. Then, the single answer panel fulfilling these criteria need to be selected.

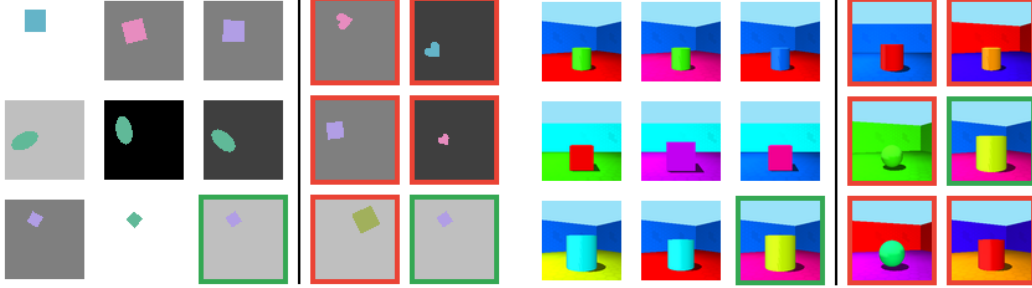


Figure 18: Answers to the examples of the RPM-like abstract visual reasoning tasks.

Figures 19 and 20 contain additional examples (including answers) of the visual reasoning tasks for each data set respectively.

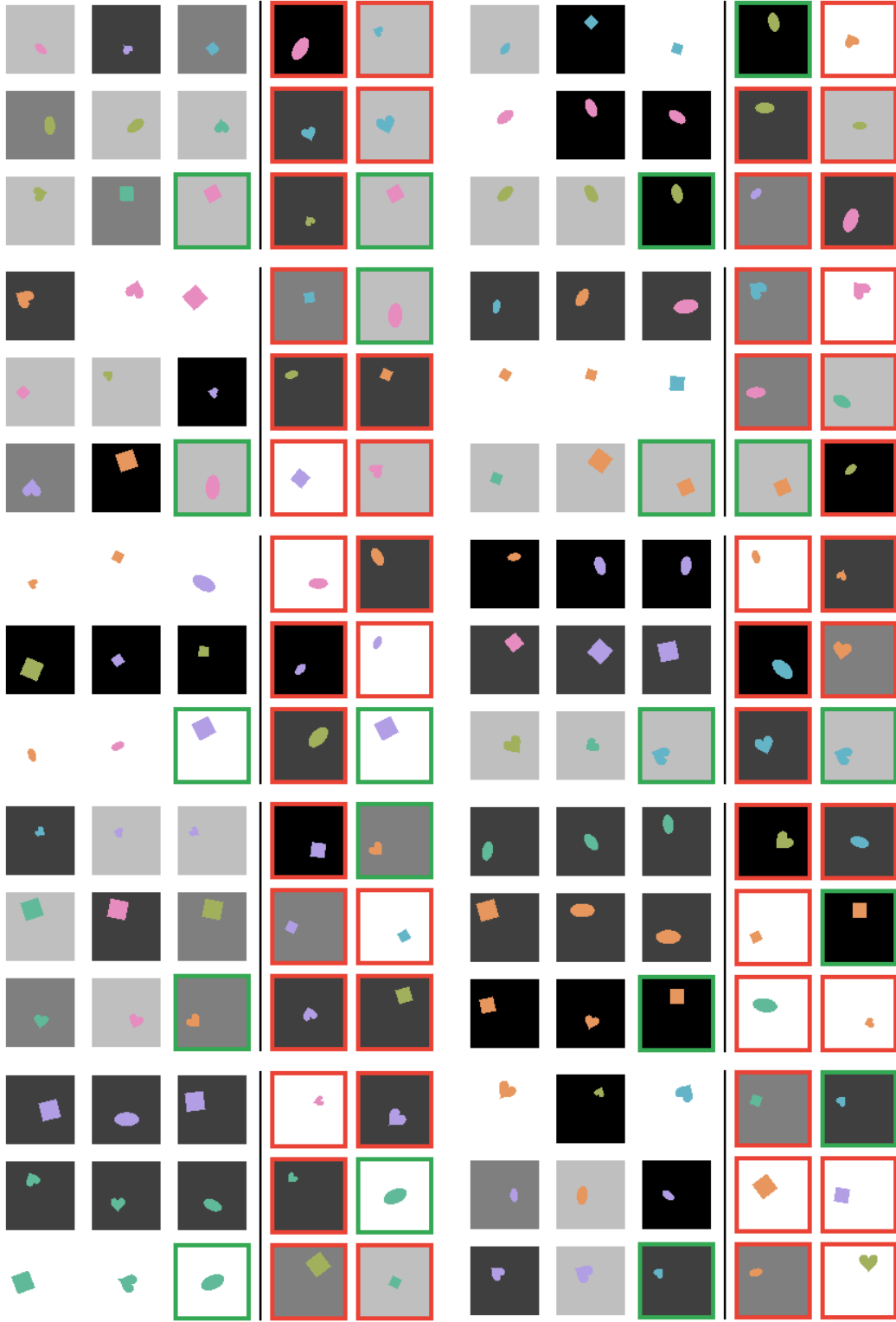


Figure 19: Additional examples (including answers) of the RPM-like abstract visual reasoning task using *dSprites*.

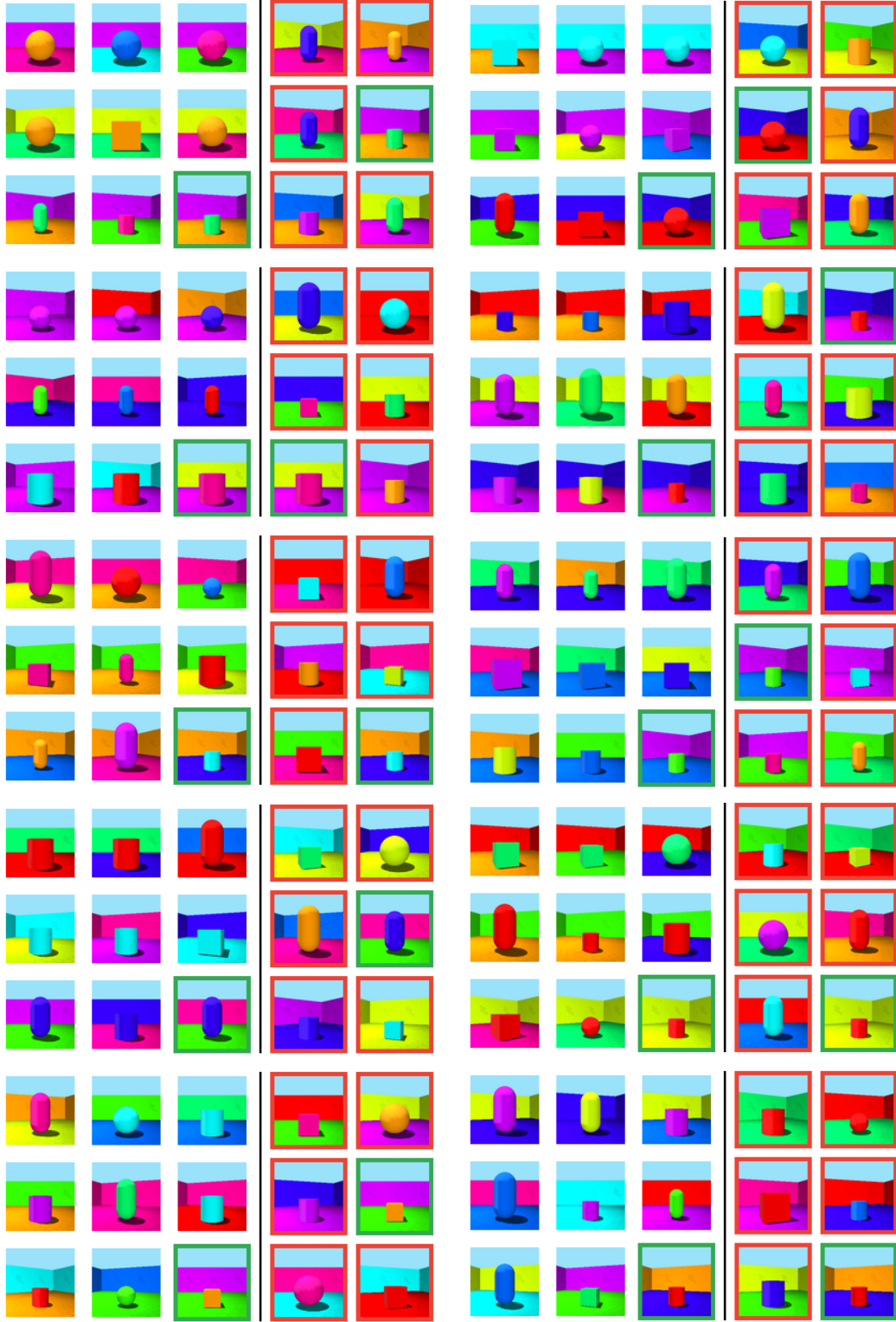


Figure 20: Additional examples (including answers) of the RPM-like abstract visual reasoning task using *3dshapes*.